Biomaterials Translational

Optimization and biocompatibility analyses of fused filament fabrication-printed polylactic acid-silicon nitride scaffolds with enhanced mechanical properties

Lovin K. John[1], Ramu Murugan[1]*, Sarat Singamneni[2], and Banu Pradheepa Kamarajan[3]

ABSTRACT

Fused filament fabrication (FFF) in additive manufacturing has emerged as a potential technology in the development of tissue engineering scaffolds of precise, complex geometries. The choice of material and process parameters is significant in determining their properties, such as mechanical strength. Polymer-ceramic composites with exceptional bioactivity have the potential for FFF applications in fabricating scaffolds. In this study, polylactic acid (PLA) composite scaffolds reinforced with silicon nitride (Si_3N_4) particles in various weight ratios (97:03, 95:05, and 93:07 weight%) were developed using FFF technology. Taguchi's orthogonal array and grey relational analysis were employed to optimize three parameters (polymer-reinforcement ratio, infill density, and layer thickness) to analyze mechanical strength – through tensile, compressive, flexural, and impact tests – surface morphology using scanning electron microscopy, and biocompatibility through 3-(4,5-dimethylthiazol-2-yl)-2,5-diphenyltetrazolium bromide (MTT assay). The optimal formulation of 95:05 wt.%, 0.17 mm layer height, and 100% infill density demonstrated superior mechanical properties with a tensile strength of 47.52 MPa, flexural strength of 67.3 MPa, compressive strength of 71.57 MPa, and impact strength of 2.63 kJ/m^2. Analysis of variance revealed layer thickness as the most influential factor (41.7%) impacting mechanical properties, followed by PLA: Si_3N_4 ratio and infill density. MTT assay and immunofluorescent staining analysis revealed that the optimal formulations enhanced cell viability and proliferation compared to controls.

Keywords:
Polymer ceramic composite; Fused filament fabrication; Grey relational analysis; Biocompatibility; Mechanical properties; Taguchi orthogonal array

***Corresponding author:**
Ramu Murugan,
m_ramu@cb.amrita.edu

How to cite this article:
John LK, Murugan R, Singamneni S, Kamarajan BP. Optimization and biocompatibility analyses of fused filament fabrication-printed polylactic acid-silicon nitride scaffolds with enhanced mechanical properties. *Biomater Transl.* 2025, 6(2), 212-222.

doi: 10.12336/bmt.25.00014

1. Introduction

Additive manufacturing technologies, especially fused filament fabrication (FFF), have revolutionized the manufacturing of customized parts for a wide range of industrial applications. The ease of processing and reduced cost of production have increased the demand for FFF in manufacturing polymers, such as polylactic acid (PLA), acrylonitrile butadiene styrene, low-density polyethylene, and nylon 6. As a biodegradable polymer derived from natural sources, such as maize starch and sugarcane, PLA has immense scope in specific applications demanding biocompatible characteristics. However, applications are limited by lower mechanical performance and surface quality, which could be improved by including suitable reinforcements such as fibers (glass fibers and carbon fibers) and micro- and nano-sized particles such as glass beads, copper, aluminum, and tungsten.[1-8] However, the inclusion of ceramic particles – such as graphene oxide, Bakelite, barium titanate, titanium dioxide, boron nitride, zirconium dioxide, silicon dioxide, silicon nitride (Si_3N_4), and silicon carbide – in PLA, acrylonitrile butadiene styrene, low-density polyethylene, etc., has exhibited a more profound influence in

enhancing the mechanical behavior and thermal stability of the composite structures.[9-22]

Implementing polymer-ceramic composites instead of polymer biomaterials and ceramic biomaterials in bone grafting has considerably enhanced the possibilities of achieving complex designs with improved mechanical strength, as well as superior osteoinductive and osteoconductive effects.[23] Composites based on ceramic-biopolymer systems, such as bioactive glass, hydroxyapatite, tricalcium phosphate, magnesium phosphate ceramics, and collagen-reinforced polymers, demonstrate improved cell viability, mechanical strength, and drug release profiles.[24,25] Biocompatible PLA composite systems with suitable surface morphology, enhanced mechanical properties – such as tensile strength, elastic modulus, and compression strength – biodegradability, and thermal stability have gained much importance in the development of bone scaffolds used in treating conditions such as osteoporosis.[26-28] However, considering *in vivo* applications, conditions for better vascularization and cell infiltration in the scaffold become more predominant factors than other properties.[27]

Composite materials fabricated using combined techniques, such as freeze-drying, electrospinning, and three-dimensional (3D) printing, have also been instrumental in developing tailor-made scaffolds with enhanced mechanical, biological, and physicochemical properties.[29,30] Among the various additive manufacturing technologies used to fabricate scaffolds, FFF technology presents greater demand as it is cheaper, requires no solvents, and produces porous surface features in printed parts that facilitate easier and more efficient cell adhesion and proliferation.[31,32] Therefore, it is quite significant to optimize the composition and manufacturing process parameters to enhance mechanical properties, surface morphology, and biocompatibility of the polymer composite specimens for developing efficient scaffolds for biological systems.[33-35] Taguchi optimization technique using analysis of variance (ANOVA) has been commonly employed for optimizing process parameters such as layer thickness, print speed, infill pattern, and build orientation for analyzing the yield strength, flexural strength, impact strength, modulus of elasticity, and rigidity modulus of the FFF-printed parts.[1,36-41]

The extensive literature survey identified the need to develop a biocompatible polymer-ceramic composite system with enhanced mechanical performance to fabricate complex designs using FFF technology. The objective of the study is to develop FFF-printed PLA-based composites reinforced with Si_3N_4 particles in three weight ratios (97:03, 95:05, and 93:07), and to optimize the print parameters for improved mechanical strength and biocompatibility. Using Taguchi's L_9 orthogonal array design and grey relational analysis (GRA), the study optimized three parameters – polymer-reinforcement ratio, infill density, and layer thickness – to achieve enhanced tensile, flexural, compressive, and impact strengths. The cell viability and biocompatibility of the fabricated scaffolds were analyzed using the colorimetric method, 3-(4,5-dimethylthiazol-2-yl)-2,5-diphenyltetrazolium bromide (MTT) assay, and immunofluorescence staining. The surface morphology was analyzed using the scanning electron microscopy (SEM) technique to determine the parameters favorable for proper cell infiltration and proliferation. Through the incorporation of Si_3N_4 particles into the PLA matrix and optimization of the process parameters, the study bridges the research gap identified by developing a composite material that combines the processability and biodegradability of PLA with the enhanced mechanical properties and potential bioactivity of Si_3N_4.

2. Materials and methodology

2.1. Development of composite pellets

The polymer-ceramic composites for this study were fabricated using the bio-based polymer PLA 3052 D from Naturtec Biopolymers (India) as the base matrix material, and α-phase silicon nitride powder particles of 95% purity with particle size <10 μm from Alfa-Aesar (Wardhill, United States) as the reinforcement. Ten kilograms of PLA and 500 g of silicon nitride were procured and then mixed in three weight ratios: 97:03, 95:05, and 93:07 wt.% based on the information extracted from the literature review.[21] The mixtures of polymer-ceramic composites in the preset weight ratios were pre-heated using the M/s Labline hot air oven (Labline Equipment, India) at a temperature of 65°C for 12 h for simple compounding and removal of absorbed moisture from the composite pellets before extrusion. The composite pellet blends were further compounded into a polymer-ceramic composite filament of 1.75 ± 0.05 mm using a single-screw extruder M/s Zv 20 (SPECIFIQ, India) as shown in **Figure 1A** and **B**.

2.2. Design of experiments

The experimental design used Taguchi's orthogonal L_9 design with three parameters and at three levels each, as shown in **Table 1**. The array contained nine experimental trials, including three columns with the factors under investigation, as shown in **Table 2**.[42] The critical experimental factors considered were weight percentage (A), layer thickness (B), and infill percentage (C). The test specimens were fabricated as per the American Society for Testing and Materials (ASTM) standards D638, D790, D695, and D256, followed by post-processing and testing for mechanical properties. The data generated was then used to identify the optimum process parameters for specific responses.

2.3. Fabrication of test specimens per the experimental design

Initially, the specimens were modeled using SOLIDWORKS (Dassault Systèmes, United States), and then sliced and

[1]Department of Mechanical Engineering, Amrita School of Engineering, Amrita Vishwa Vidyapeetham, Coimbatore, Tamil Nadu, India; [2]Department of Mechanical Engineering, School of Engineering, Auckland University of Technology, Auckland, New Zealand; [3]Department of Biotechnology, PSG College of Technology, Coimbatore, Tamil Nadu, India

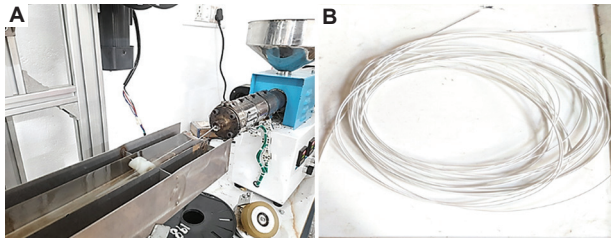

Figure 1. Extrusion of polylactic acid-silicon nitride composite filament for three-dimensional printing. (A) Extrusion setup and (B) the extruded filament.

converted into G-codes using a slicing software, Simplify3D (version 4.1.2 Simplify3D, United States). They were later saved as.stl files for 3D printing. An open-source FFF 3D printer INFILL CUBE C300 (Infillcube, India) with a dimensional accuracy of ±0.01 mm was utilized for fabricating test specimens. The experimental design for each combination of the L_9 orthogonal array and manufacturing process parameters used for 3D printing are presented in **Tables 2** and **3**, respectively. A quasi-isotropic raster layup, $[45°/0°/-45°/90°]_s$, was selected based on previous studies conducted,[21] and the samples of test specimens fabricated using the experimental design are shown in **Figure 2A** and **B**. A total of 120 samples were printed for the experimental analysis.

2.4. Mechanical characterization of test specimens

The specimens were tested for tensile, compressive, flexural, and impact properties according to ASTM D638, D695, D790, and D256, respectively. The tensile test, compressive test, and flexural tests were conducted utilizing HT 50 KL Tinius Olsen Universal Testing Machine (Tinius Olsen India Private Limited, India) at crosshead speeds of 5 and 1.3 mm/min, respectively. The three-point bending flexural test involves applying a center load on a supported system. Impact tests were used to analyze the energy absorption of the notched 3D printed samples, using the Tinius Olsen IT 504 series Izod Impact Tester (Tinius Olsen India Private Limited, India). Surface morphological analysis of fractured tensile specimens of the highest mechanical strength was conducted through SEM using Gemini 300 FESEM (Zeiss, Germany) with a resolution of 2 nm. The maximum voltage used was 15 kV to capture sample surface images at a magnification of ×5,000.

2.5. Optimization using grey scale analysis

In this study, GRA was used to determine the optimal combination of independent variables yielding superior mechanical properties. The experimental data were initially normalized for grey relational generation, ranging from zero to one. The normalization approach was tailored to the response variable characteristics. For this investigation, the "higher is better" concept was adopted, as maximizing all studied mechanical properties was crucial for optimal performance enhancement, and was calculated using Equation I.

$$x_{ij} = \frac{y_{ij} - min(y_{ij})}{max(y_{ij}) - min(y_{ij})} \quad \text{(I)}$$

Table 1. Levels and parameters used in Taguchi's orthogonal array

Parameters	Levels		
	1	2	3
Weight percentage of silicon nitride (%)	3	5	7
Layer thickness (mm)	0.13	0.15	0.17
Infill percentage (%)	100	95	90

Table 2. Orthogonal L_9 array based on Taguchi's method

Run	Weight percentage of silicon nitride (%)	Layer thickness (mm)	Infill percentage (%)
A_1	3	0.13	100
A_2	3	0.15	95
A_3	3	0.17	90
B_1	5	0.13	95
B_2	5	0.15	90
B_3	5	0.17	100
C_1	7	0.13	90
C_2	7	0.15	100
C_3	7	0.17	95

Table 3. Design and manufacturing parameters employed in three-dimensional printing

No.	Description	Values
1	Layer height (mm)	0.13, 0.15, 0.17
2	Bed temperature (°C)	65
3	Print speed (mm/s)	40
4	Raster angle (°)	$[45°/0°/-45°/90°]_s$
5	Material	Polylactic acid-silicon nitride composite
6	Nozzle diameter (mm)	0.4 mm
7	Nozzle temperature (°C)	210
8	Infill percentage (%)	90, 95, 100
9	Filament diameter (mm)	1.75±0.05

Where, x_{ij} represents the normalized data and y_{ij} represents the corresponding measured data point, max (y_{ij}) is the maximum value of y_{ij}, and min (y_{ij}) is the minimum value of y_{ij}.

The assessment of the deviation sequence of normalized data is necessary to compute grey relational coefficients (GRC) and is determined by the absolute difference between the highest normalized value, which is calculated using Equation II,

$$\Delta_{oi}(k) = x_o(k) - x_i(k) \quad \text{(II)}$$

Where $\Delta_{oi}(k)$ represents deviation, $x_o(k)$ represents the largest normalized value of the output and $x_i(k)$ represents the normalized value of the output variable in the i^{th} experiment.

The GRC value for each variable in this study is determined using Equation III, with the distinguishing coefficient (ϕ) set uniformly at 0.5 for all mechanical strength parameters. The grey relational grade (GRG) for each response is computed using Equation IV, while the rank of each performance characteristic is determined. The mean GRG is calculated for every level of all factors in the orthogonal array to determine the best values of input variables for maximizing mechanical

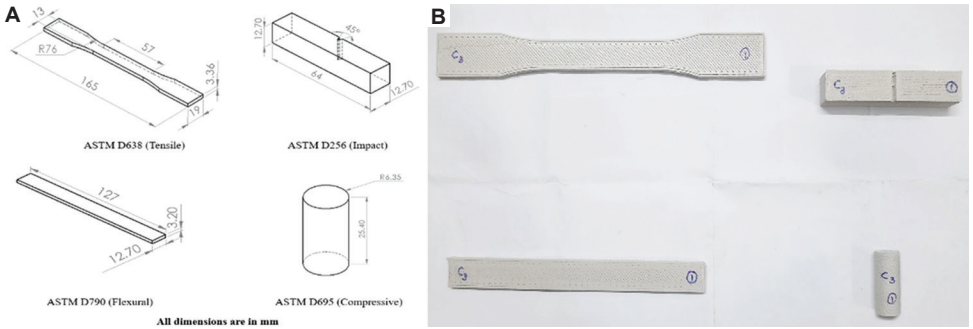

Figure 2. Design and model of test specimens. (A) Standard test specimens and (B) three-dimensionally printed test specimens according to Taguchi's L_9 experimental design.
Abbreviation: ASTM: American Society for Testing and Materials.

properties. ANOVA was conducted to assess the impact of each input parameter on the mechanical properties.

$$\varepsilon_i(k) = \frac{\Delta + (\varphi^* \Delta max)}{\Delta_{ij} + (\varphi^* \Delta max)} \quad \text{(III)}$$

Where, Δ and Δmax are the smallest and largest values, respectively, of the series of deviation sequence responses, ϕ is the distinguishing coefficient, and Δ_{ij} represents the corresponding data points from the deviation sequence responses.

$$\gamma_i = \frac{1}{n}\sum_{i=1}^{n} \varepsilon_i(k) \quad \text{(IV)}$$

2.6. Biocompatibility studies of polymer composite scaffolds

2.6.1. MTT assay

The MTT assay, a colorimetric method called MTT, is utilized for evaluating cell viability, proliferation, and cytotoxicity. It is based on the concept that metabolically active cells have mitochondrial dehydrogenase enzymes that can convert a yellow tetrazolium salt, MTT, into purple formazan crystals. The quantity of formazan generated is directly proportional to the number of viable cells present.

The PLA/Si_3N_4 composite scaffolds, fabricated according to the design of experiments discussed above, were cut into rectangular specimens and sterilized in an autoclave at 120°C and 15 psi pressure for 15 min. These scaffolds were then immersed in Dulbecco's modified Eagle's medium (DMEM-AL007S, HiMedia, India), a modified basal medium for cellular proliferation, and seeded with human osteosarcoma cell line (MG63), obtained from the National Centre for Cell Science, India. The DMEM was supplemented with 200 mM L-glutamine, 10% fetal bovine serum, and 1× antibiotic-antimycotic solution (A002, HiMedia, India). The cells were incubated with 5% CO_2 at 37°C and subsequently trypsinized. The sterilized scaffolds were then seeded with 1 mL of the medium with 1 × 10^4 cells in a 48-well plate for 24 h. Cell viability was assessed using the MTT assay. After adding the MTT solution to the wells, the plates were incubated for about 4 h to allow formazan crystal formation. Subsequently, it was removed from the well, aspirated, and dissolved in dimethyl sulfoxide to yield a uniform purple solution. Absorbance was measured at 570 nm using a multi-well plate reader. The control samples, consisting of the cell lines without the scaffold material, were treated and analyzed similarly. SEM was employed to capture images of the scaffolds for evaluating cell growth and other microstructural details.

2.6.2. Immunofluorescent staining

Immunofluorescent staining employs specific antibodies conjugated to fluorescent markers to detect cellular proteins and assess biocompatibility responses. This technique enables the visualization of inflammatory markers, cell viability, and tissue responses at implant-material interfaces. Fluorescent imaging provides quantitative analysis of cellular responses, offering sensitive detection of biocompatibility parameters essential for medical device evaluation.

For fluorescent staining, the autoclaved scaffolds of Run 6 were incubated with 1 × 10^4 cells in a 6-well plate for 48 h. After incubation, the used media was replaced with sterile phosphate-buffered saline of pH 7.4. To visualize the cells, SYTO 9 dye (Thermo Fisher Scientific, India) and propidium iodide stain (Thermo Fisher Scientific, India) in a 1:1 ratio were added per the manufacturer's protocol (Live/Dead BacLight, Invitrogen L7012, Thermo Fisher Scientific, India). To further confirm the concentration of live cells, 4',6-diamidino-2-phenylindole (DAPI; Thermo Fisher Scientific, India) stain was used, staining the nucleus of the live cells. The dyes were added to the cells and incubated in the dark for 10 min before being visualized under a Nikon Ti Eclipse fluorescent microscope (Nikon Instruments Inc., United States).

3. Results and discussion

3.1. Mechanical strength analysis

The mechanical characterization of the PLA/Si_3N_4 composites, including tensile, flexural, impact, and compressive tests, was conducted. A detailed analysis of the various compositions and parameters of the L_9 orthogonal array is presented in **Table 4**. The detailed study of the different compositions, processing conditions, and their corresponding mechanical strengths revealed that the PLA-Si_3N_4 (95:05) B_3 formulation consistently exhibited superior performance across various mechanical properties. The optimized composition exhibited superior mechanical properties, with peak values in tensile strength (47.52 MPa), flexural strength (67.3 MPa),

compressive strength (71.57 MPa), flexural modulus (3140 MPa), and impact strength (2.63 kJ/m²). The enhanced mechanical characteristics are attributed to effective stress transfer, optimal particle distribution, and strong interfacial adhesion. Comparing composites with 97:03, 95:05, and 93:07 ratios indicated that increased Si_3N_4 content was instrumental in improving strength values in conjunction with the effects of the process parameters. These findings demonstrate the importance of optimizing the mechanical properties of PLA/Si_3N_4 composites in various applications.

3.1.1. Tensile strength

The tensile strength of PLA composites reinforced with Si_3N_4 particles is shown in **Figure 3**. The values for tensile strength of polymer-ceramic composites, which is a measure of maximum stress endured before fracture, varied from 35.45 MPa to 47.52 MPa, and the tensile modulus value ranged from 2,250 MPa and 2,920 MPa, as indicated in **Table 4**.

The PLA-Si_3N_4 composite with a ratio of 95:05 (B_3) exhibited the highest tensile strength of 47.52 MPa. The optimal composition of the PLA-Si_3N_4 sample appears to be around 5 wt.%. The SEM images also validated the enhancement of tensile strength of the polymer ceramic composite specimen at 95:05 wt.% compared to the other two combinations.

In **Figure 4**, the failure mode exhibited both ductile and brittle characteristics. Smooth and flat regions exhibited brittle fracture, while minor deformations and irregularities on the surface indicated ductile behavior. Compared with other weight combinations, the 93:07 wt.% composition (**Figure 4C**) showed additional pull-out sites for the reinforced particle during fracture compared to other compositions, resulting in a decrease in tensile strength. Similarly, **Figure 4B** illustrates that the close connection between the matrix and particle filler resulted in a strong interfacial adhesion, promoting efficient load transfer and consequently increasing tensile strength than other weight ratios.

3.1.2. Flexural strength

The flexural strength of various PLA composites enhanced with Si_3N_4 particles is shown in **Figure 5**. Flexural strength measures the ability to withstand deformation when subjected to loads. Flexural strength values of the polymer ceramic composite varied from 54.3 MPa to 67.3 MPa, and flexural modulus varied from 2,303 MPa to 3,233 MPa (**Table 4**).

The PLA-Si_3N_4 composite with a ratio of 95:05 (B_3) showed the greatest flexural strength at 67.30 MPa. The enhanced strength could be attributed to effective stress transfer between the matrix and the reinforcement, as well as to potential

Table 4. Consolidated mechanical strength analysis based on L_9 orthogonal array

Run	Material composition (ratio)	Tensile strength (MPa)	SD	Tensile modulus (MPa)	SD	Flexural strength (MPa)	SD	Flexural modulus (MPa)	SD	Impact strength (kJ/m²)	SD	Compressive strength (MPa)	SD
A_1	PLA+$Si_3N_{4(97:03)}$	40.61	0.71	2,463	84.85	64.25	5.44	3,233	365.6	2.39	0.18	62.23	2.89
A_2	PLA+$Si_3N_{4(97:03)}$	43.08	5.08	2,920	92.01	63.27	3.93	3,017	233.4	2.36	0.07	62.25	8.00
A_3	PLA+$Si_3N_{4(97:03)}$	44.19	3.33	2,587	58.30	64.30	8.34	2,497	380.0	2.44	0.03	60.73	5.30
B_1	PLA+$Si_3N_{4(97:03)}$	39.75	2.19	2,250	28.28	59.67	4.60	2,850	222.7	2.25	0.01	59.27	5.20
B_2	PLA+$Si_3N_{4(97:03)}$	42.75	2.51	2,577	43.30	54.30	2.55	2,303	179.5	2.35	0.07	61.90	6.43
B_3	PLA+$Si_3N_{4(97:03)}$	47.52	1.61	2,517	70.71	67.30	6.38	3,140	183.8	2.63	0.37	71.57	3.14
C_1	PLA+$Si_3N_{4(97:03)}$	35.45	0.83	2,300	91.65	54.60	4.13	2,467	170.1	2.24	0.20	57.90	4.67
C_2	PLA+$Si_3N_{4(97:03)}$	35.75	3.70	2,395	43.10	59.90	3.08	2,590	149.5	2.23	0.60	60.80	3.98
C_3	PLA+$Si_3N_{4(93:07)}$	38.27	1.54	2,540	63.60	61.20	9.19	2,790	240.4	2.53	0.02	59.00	2.40

Abbreviations: PLA: Polylactic acid; SD: Standard deviation; Si_3N_4: Silicon nitride.

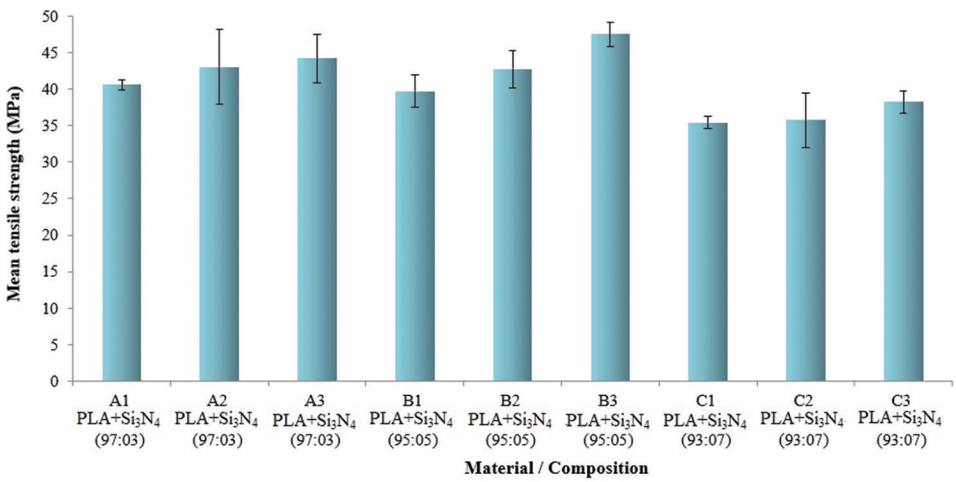

Figure 3. Tensile strength of polylactic acid-silicon nitride (Si_3N_4) composite based on experimental design combinations

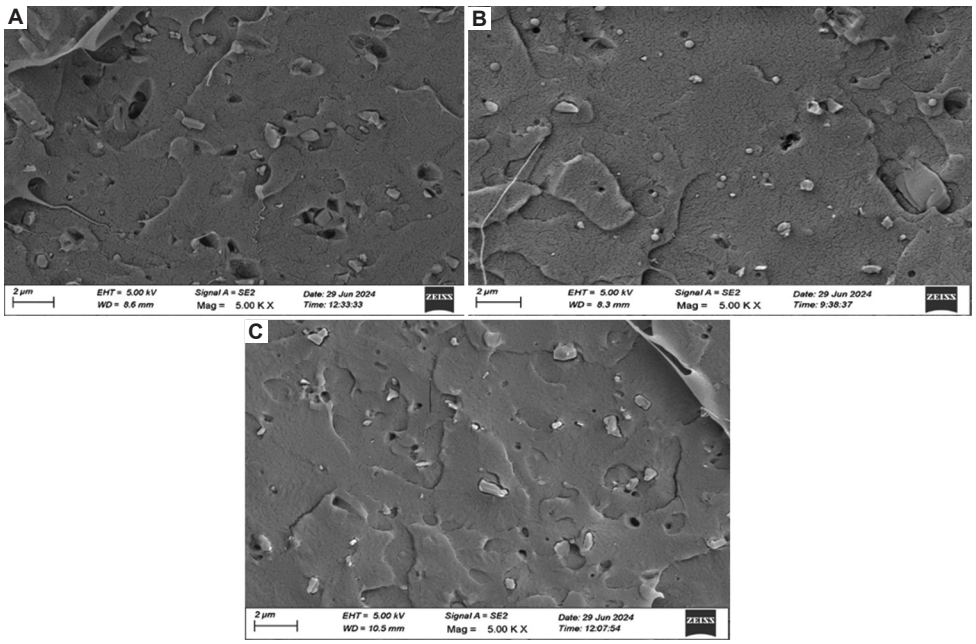

Figure 4. Scanning electron microscope images of polylactic acid-silicon nitride composite samples with combination (A) 97:03 (A_3), (B) 95:05 (B_3), and (C) 93:07 (C_3). Scale bar: 2 µm, magnification: 5,000×.

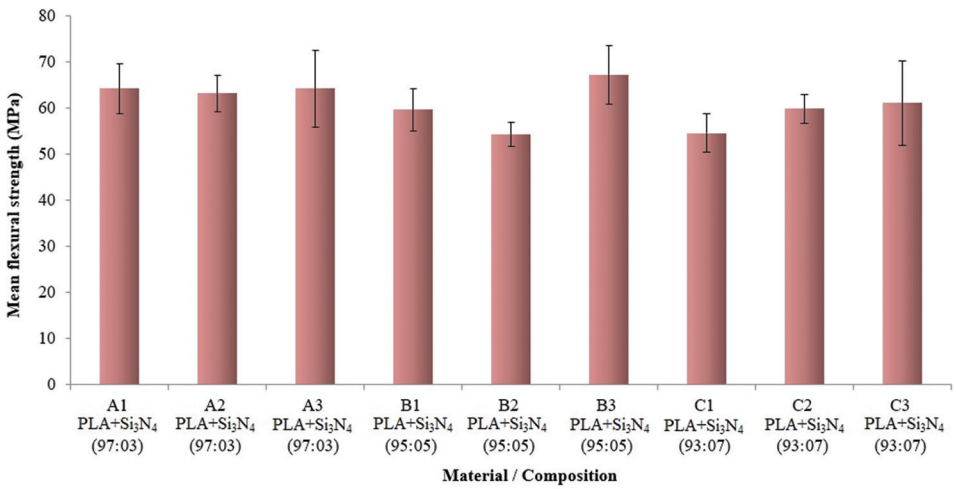

Figure 5. Flexural strength of polylactic acid-silicon nitride (Si_3N_4) composite based on experimental design combinations

improvements in interfacial adhesion. The compositions (97:03) and (95:05) revealed that strength does not increase uniformly with increasing Si_3N_4 content. This non-linear correlation indicates that once a critical concentration of Si_3N_4 is reached, adding more may not yield additional advantages. The best ratio seems to be approximately 5 wt.% for the PLA-Si_3N_4 sample, exhibiting improved strength and stiffness.

3.1.3. Compressive strength

The compressive strengths of PLA composites reinforced with Si_3N_4 particles are shown in **Figure 6**, with values ranging between 57.9 and 71.57 MPa, as noted in **Table 4**. The strength range of the 95:05 composition was higher than that of the 97:03 composition. The B_3 PLA-Si_3N_4 (95:05) sample achieved the highest compressive strength of 71.57 MPa, attributed to effective load transfer, improved interfacial adhesion, optimal particle distribution, and potential densification. Furthermore, the presence of Si_3N_4 particles may reduce polymer chain mobility, thereby influencing the compressive properties.

3.1.4. Impact strength

Figure 7 provides the analysis of impact strength in PLA composites reinforced with Si_3N_4 particles. The impact strength values of polymer ceramic composite varied from 2.23 to 2.63 kJ/m^2 across various compositions and processing conditions. The (95:05) compositions exhibited the highest impact strength range compared to the 97:03 composition. The PLA-Si_3N_4 (95:05) B_3 sample achieved the highest impact strength of 2.63 kJ/m^2, suggesting an optimal balance between the ductile PLA matrix and rigid Si_3N_4 reinforcement particles. This enhancement likely resulted from effective energy dissipation mechanisms, improved interfacial adhesion, and optimal particle distribution, leading to crack deflection and energy absorption.

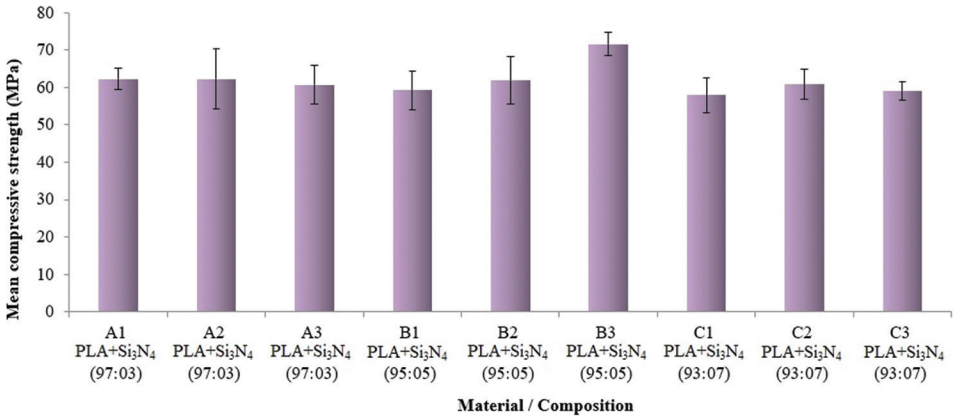

Figure 6. Compressive strength of polylactic acid-silicon nitride (Si_3N_4) composite based on experimental design combinations

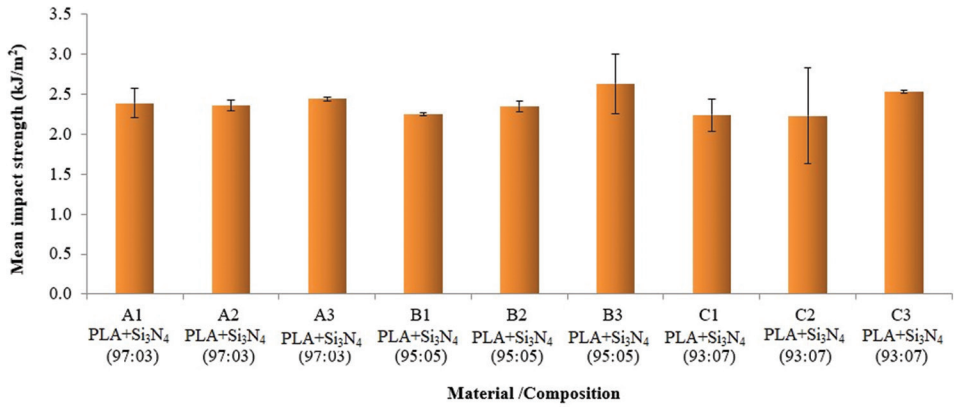

Figure 7. Impact strength of polylactic acid-silicon nitride (Si_3N_4) composite based on experimental design combinations

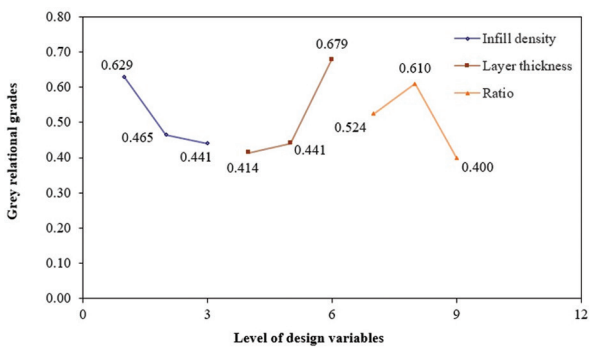

Figure 8. Grey relational grade based on design variables

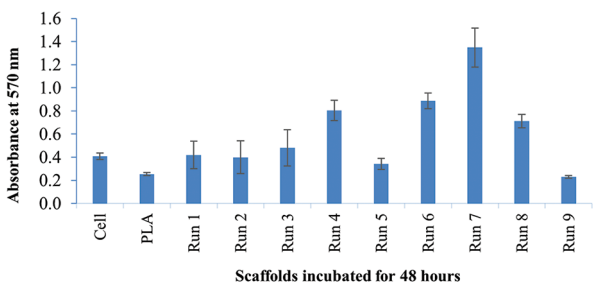

Figure 9. 3-(4,5-dimethylthiazol-2-yl)-2,5-diphenyltetrazolium bromide assay of the polymer ceramic composite scaffolds
Abbreviation: PLA: Polylactic acid.

3.2. Process parameters optimization

A Taguchi L_9 orthogonal array design, consisting of nine experimental runs, was employed to simultaneously optimize various objective characteristics using GRA. Based on Section 2.5, the normalized experimental data and respective deviation sequences (delta) were analyzed using Equations I and II, respectively. The "higher is better" criterion was selected for analysis of mechanical properties. **Table 5** illustrates the calculated GRC using Equation III, GRG using Equation IV, and their respective rankings for each performance characteristic. Thus, the multi-response optimization problem was consolidated into a single, equivalent objective function for analysis.

Analysis of the data presented in **Table 5**, derived from the Taguchi method, revealed that geometric patterns exert a substantial influence on the mechanical properties of the printed composites. The mechanical properties were influenced by the layer thickness during printing more than the infill density, but less than the reinforcement weight ratio. The experimental run 6 exhibited the highest GRC, indicating optimal input variable combinations. Run 6 comprised a 95:05 wt.% ratio of PLA to Si_3N_4, a layer thickness of 0.17 mm, and 100% infill density. The better the performance, the higher the GRG.

Table 6 and **Figure 8** present the mean GRG ratio for each level of the process parameters, useful to indicate the optimal

Table 5. Grey relational coefficients, grey relational grade, and rank for each performance based on the L_9 orthogonal array

Run	Parameters			Tensile strength			Compressive strength			Flexural strength			Impact strength			Mean GRC	Grey relational grade	Rank
	Ratio	Layer thickness	Infill density	Normalized value	Delta	GRC	Normalized value	Delta	GRC	Normalized value	Delta	GRC	Normalized value	Delta	GRC			
1	3	0.13	100	0.43	0.57	0.47	0.32	0.68	0.42	0.32	0.68	0.42	0.4	0.6	0.46	0.506	0.256	4
2	3	0.15	95	0.63	0.37	0.58	0.32	0.68	0.42	0.32	0.68	0.42	0.33	0.68	0.43	0.510	0.261	3
3	3	0.17	90	0.72	0.28	0.64	0.21	0.79	0.39	0.21	0.79	0.39	0.53	0.48	0.51	0.557	0.310	2
4	5	0.13	95	0.36	0.64	0.44	0.13	0.87	0.36	0.13	0.87	0.36	0.05	0.95	0.35	0.401	0.161	7
5	5	0.15	90	0.6	0.4	0.56	0.29	0.71	0.41	0.29	0.71	0.41	0.3	0.7	0.42	0.431	0.185	6
6	5	0.17	100	1	0	1.00	1	0	0.99	1	0	0.99	1	0	1.00	0.999	0.997	1
7	7	0.13	90	0	1	0.33	0	1	0.33	0	1	0.33	0.03	0.97	0.34	0.336	0.113	9
8	7	0.15	100	0.02	0.98	0.34	0.21	0.79	0.39	0.21	0.79	0.39	0	1	0.33	0.382	0.146	8
9	7	0.17	95	0.23	0.77	0.40	0.08	0.92	0.35	0.08	0.92	0.35	0.75	0.25	0.67	0.482	0.233	5

Abbreviations: GRC: Grey relational coefficient.

Table 6. Average grey relational grade ratio for each process parameter level

Factors	Mean grey relational grade			Maximum-minimum	Rank
	Level 1	Level 2	Level 3		
Ratio	0.524	0.610	0.400	0.210	2
Layer thickness	0.414	0.441	0.679	0.265	1
Infill density	0.629	0.465	0.441	0.188	3

input variable values for maximizing mechanical properties. Analysis of these mean GRG revealed that the optimal parametric combination for achieving superior multiple performance characteristics is A2-B3-C1. An examination of the GRG data was performed using ANOVA, and the findings are shown in **Table** 7.

ANOVA was employed to quantify the contribution of individual input parameters to the mechanical properties, as shown in **Table** 7. This analysis showed that the ratio, layer height, and infill percentage were the most important factors for improving mechanical strength. The results indicated that layer thickness contributed the most substantial influence (41.7%), followed by the ratio of reinforcement (21.8%), while infill density exhibited the least impact (20.5%) on the mechanical properties.

To further examine the data with the Taguchi model, the GRC of the output parameters was computed, and all nine specimens were ranked from best to worst based on a grade assigned to each specimen.

3.3. Biocompatibility analysis

3.3.1. MTT assay

The MTT assay results presented in **Figure 9** offer valuable insights into the performance of various scaffold conditions for cell culture over a 48-h incubation period. The data revealed a complex landscape of cell viability and proliferation across nine experimental runs, with notable variations in absorbance at 570 nm, indicative of mitochondrial activity. The baseline cell MG63 condition, likely representing standard culture conditions, showed a moderate absorbance of approximately 0.4 at 570 nm. This acted as a reference point for evaluating the performance of the experimental scaffold conditions. Experimental Runs 3, 4, 6, and 7 demonstrated absorbance values surpassing the cell control, indicating enhanced cellular viability and proliferation. Run 7 demonstrated exceptional performance with an absorbance of approximately 1.4, indicating a potential 2.3-fold increase in cellular activity compared to the control. This significant enhancement may be due to improved cell adhesion, favorable surface chemistry promoting cell spreading, optimal porosity facilitating nutrient diffusion, or the presence of bioactive cues that stimulate cellular metabolism and proliferation. Conversely, the lower or comparable absorbance relative to the cell control in some runs may be due to the heterogeneous cell distribution within the scaffolds, localized differences in scaffold properties, or variations in nutrient and oxygen availability throughout the 3D structure. The findings from this study have significant implications for scaffold design in tissue engineering

Table 7. Analysis of variance for grey relational grade

Factors	SSQ	DOF	MSQ	Contribution	*F* ratio$_{(calculated)}$	*F*-value	Remarks
Ratio	0.067	2	0.033	0.218	5.48	4.46	Significant
Layer thickness	0.128	2	0.064	0.417	10.47	4.46	Significant
Infill density	0.063	2	0.031	0.205	5.14	4.46	Significant
Error	0.049	8	0.006	0.161			
SST				0.307			

Abbreviations: DOF: Degree of freedom; MSQ: Mean square; SSQ: Sum of squares; SST: Sum of squares total.

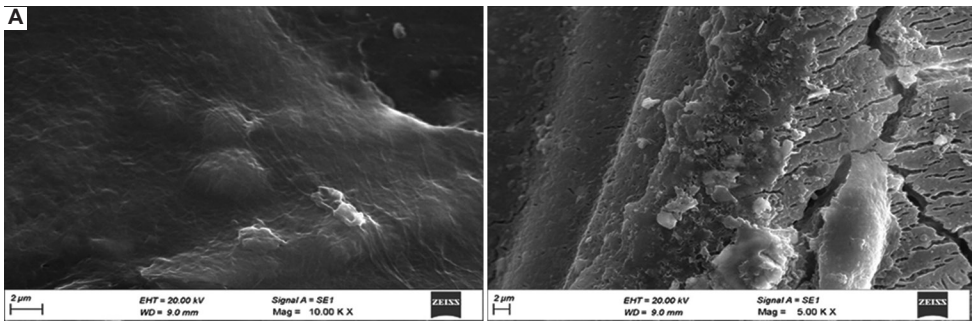

Figure 10. Scanning electron microscopy image of the interface between cells and the polymer-ceramic composite scaffolds in Run 6 combination. Scale bar: 2 µm, magnifications: (A) 10,000× and (B) 5,000×.

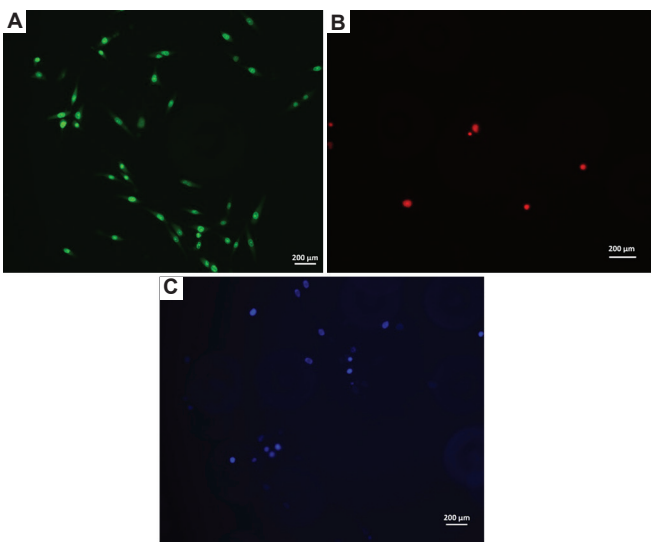

Figure 11. The fluorescent images of the cells stained with (A) SYTO 9 (green), (B) propidium iodide (red), and (C) 4',6-diamidino-2- phenylindole staining (DAPI) (blue). Scale bar: 200 µm, magnification: 20×.

applications. The identification of conditions of Run 6 that substantially enhance cellular activity offers promising avenues for optimizing biomaterial formulations to support tissue regeneration.

Figure 10A reveals the extracellular matrix deposition with attached cells showing an elongated morphology. These thin, filament-like projections represent excellent cellular adhesion to the substrate. **Figure 10B** demonstrates the broader topographical features of the scaffold surface with significant cell infiltration within the microporous morphology. The roughness and irregularity of the surface may have enhanced cell anchorage. The SEM images indicate that the polymer composite scaffolds at optimal conditions are favorable for potential bioactivity, such as cell viability and proliferation, making it a promising material for tissue engineering applications.

3.3.2. Immunofluorescent staining

Figure 11 presents the immunofluorescent staining of the cells with SYTO 9, propidium iodide, and DAPI to analyze the live and dead cells attached to the Run 6 scaffold.

The fluorescent dye SYTO 9 (green) penetrates the cells and stains the nucleic acid of live cells green, while propidium iodide stains the nucleic acid of dead cells red. Hence, green-colored cells indicate live cells, and red-colored cells indicate dead cells. For further confirmation, a DAPI stain was used, staining the nucleus of the live cells blue. The higher number of blue and green colored cells compared to the dead (red) cells in the images above indicates that the scaffold material is non-toxic and promotes cell attachment and proliferation.

4. Conclusions

Optimal process conditions for FFF of PLA-Si_3N_4 composite filaments with varying compositions have been identified through experimental evaluations based on the Taguchi L_9 design. The integration of the statistical optimization efforts, guided by Taguchi's orthogonal array design and GRA, identified the optimal composition and processing parameters for maximizing multiple mechanical properties simultaneously. The most promising formulation, consisting of a 95:05 weight% PLA to Si_3N_4 ratio, 0.17 mm layer height, and 100% infill density, exhibited the highest tensile strength (47.52 MPa), flexural strength (67.3 MPa), compressive strength (71.57 MPa), and impact strength (2.63 kJ/m^2).

The biocompatibility assessment through MTT assay revealed that experimental Runs 3, 4, 6, and 7 supported enhanced cell viability and proliferation compared to control conditions, suggesting that the incorporation of Si_3N_4 particles potentially

creates a more favorable microenvironment for cell growth and function. The immunofluorescence staining of the B3 samples confirms that the number of live cells attached is more than the number of dead cells. This suggests that the scaffold is non-toxic and favorable for successful cell proliferation. However, the experimental design was limited to 9 runs due to excessive material and production costs. Further ratios of the composite with higher reinforcement percentage could not be studied due to potential nozzle clogging. The development of these advanced polymer-ceramic composites represents a significant contribution to the field of biomaterials, especially in tissue engineering and regenerative medicine, and holds great promise for improving patient outcomes in orthopedic and dental applications.

Acknowledgement
The authors would like to acknowledge CIPET Kochi, Infill Cube-3D Printing, PSG Tech, COE-AMGT Ettimadai, and DST-STIC Kochi for successfully conducting various experiments and analyses.
Financial support
None.
Conflicts of interest statement
The authors declare that there is no conflict of interest for the present work.
Author contributions
Conceptualization: LKJ and RM; *Formal analysis*: LKJ; *Investigation*: LKJ and BPK; *Methodology*: LKJ; *Project administration*: RM and BPK; *Writing – original draft*: LKJ; *Writing – review & editing*: RM, SS, BPK. All authors have read and agreed to the published version of the manuscript.
Ethics approval and consent to participate
Not applicable.
Consent for publication
Not applicable.
Availability of data
All data analyzed have been presented in the paper.

References

1. Torrado AR, Shemelya CM, English JD, Lin Y, Wicker BR, Roberson AD. Characterizing the effect of additives to ABS on the mechanical property anisotropy of specimens fabricated by material extrusion 3D printing. *Addit Manuf.* 2015;6:16-29. doi: 10.1016/j.addma.2015.02.001
2. *Virgin PBT Fr V0 Particle Granule Pellet PBT 15% Glass Fiber Compounds.* Available from: https://keyuanplastic.en.made-in-china.com/product/saprhrfpgtcq/china-virgin-pbt-fr-v0-particle-granule-pellet-pbt-15-glass-fiber-compounds.html [Last accessed on 2024 Mar 12].
3. *Frp/Grp Grating.* 2022. Available from: https://fibertech.co.in/frp-grp-grating.html?gad_source=1&gclid=cj0kcqjw4cs-bhdgarisabg4_j0ualqmrm1fakvgfu0grmdx917n5cuc1iolsdnbzhe8frwcene3je8aavivealw_wcb [Last accessed on 2024 Mar 12].
4. Mayekar PC. *Accelerating the Biodegradation of Poly* (*Lactic Acid*) *at Mesophilic Temperatures* [dissertation]. Michigan: Michigan State University; 2024.
5. Tekinalp HL, Kunc V, Velez-Garcia GM, *et al.* Highly oriented carbon fiber-polymer composites via additive manufacturing. *Compos Sci Technol.* 2014;105:144-150. doi: 10.1016/j.compscitech.2014.10.009
6. Jayashuriya M, Gautam S, Aravinth AN, Vasanth G, Murugan R. Studies on the effect of part geometry and process parameter on the dimensional deviation of additive manufactured part using ABS material. *Prog Addit Manuf.* 2022;7(6):1183-1193. doi: 10.1007/s40964-022-00292-9
7. Amithesh SR, Shanmugasundaram B, Kamath, S, Adhithyan SS, Murugan R. Analysis of dimensional quality in FDM printed Nylon 6 parts. *Prog Addit Manuf.* 2024;9(4):1225-1238. doi: 10.1007/s40964-023-00515-7
8. Kangishwar S, Radhika N, Sheik AA, Chavali A, Hariharan S. A comprehensive review on polymer matrix composites: Material selection, fabrication, and application. *Polym Bull.* 2023;80(1):47-87. doi: 10.1007/s00289-022-04087-4
9. Aumnate C, Pongwisuthiruchte A, Pattananuwat P, Potiyaraj P. Fabrication of ABS/graphene oxide composite filament for fused filament fabrication (FFF) 3D printing. *Adv Mater Sci Eng.* 2018;1:1-9. doi: 10.1155/2018/2830437
10. Khatri B, Lappe K, Habedank M, Mueller T, Megnin C, Hanemann T. Fused deposition modeling of ABS-barium titanate composites: A simple route towards tailored dielectric devices. *Polymers* (*Basel*). 2018;10(6):666. doi: 10.3390/polym10060666
11. Divakar H, Nagaraja R, Puttaswamaiah S, Guruprasad H. Mechanical characterization of thermoplastic ABS/glass fibre reinforced polymer matrix composites. *Int J Eng Res Technol.* 2015;4:1127-1131. doi: 10.17577/IJERTV4IS051122
12. Singh R, Kumar R, Singh I. Investigations on 3D printed thermosetting and ceramic-reinforced recycled thermoplastic-based functional prototypes. *J Thermoplast Compos Mater.* 2021;34(8):1103-1122. doi: 10.1177/0892705719864623
13. Yilmazer U. Tensile, flexural and impact properties of a thermoplastic matrix reinforced by glass fiber and glass bead hybrids. *Compos Sci Technol.* 1992;44(2):119-125. doi: 10.1016/0266-3538(92)90104-B
14. Wang G, Zhang D, Li B, Wan G, Zhao G, Zhang A. Strong and thermal-resistance glass fiber-reinforced polylactic acid (PLA) composites enabled by heat treatment. *Int J Biol Macromol.* 2019;129:448-459. doi: 10.1016/j.ijbiomac.2019.02.020
15. Ranjbar M, Dehghan Noudeh G, Hashemipour MA, Mohamadzadeh I. A systematic study and effect of PLA/Al_2O_3 nanoscaffolds as dental resins: Mechanochemical properties. *Artif Cells Nanomed Biotechnol.* 2019;47(1):201-209. doi: 10.1080/21691401.2018.1548472
16. Kurtycz P, Ciach T, Olszyna A, *et al.* Electrospun poly (L-lactic) acid/nanoalumina (PLA/Al_2O_3) composite fiber mats with potential biomedical application-investigation of cytotoxicity. *Fibers Polym.* 2013;14:578-583. doi: 10.1007/s12221-013-0578-5
17. Liu W, Wu N, Pochiraju, K. Shape recovery characteristics of SiC/C/PLA composite filaments and 3D printed parts. *Compos A Appl Sci Manuf.* 2018;108:1-11. doi: 10.1016/j.compositesa.2018.02.017
18. Yu S, Kim DK, Park C, Hong SM, Koo CM. Thermal conductivity behavior of SiC-Nylon 6, 6 and hBN-Nylon 6, 6 composites. *Res Chem Intermed.* 2014;40:33-40. doi: 10.1007/s11164-013-1452-1
19. Benabid FZ, Mallem OK, Zouai F, Cagiao ME, Benachour D. Effect of the mechanical treatment of alumina on thermal, morphological and dielectric properties of LDPE/Al_2O_3 composites. *S Afr J Chem.* 2018;71:150-154.
20. Dhabale R, Jatti VS. A bio-material: Mechanical behaviour of LDPE-Al_2O_3-TiO_2. *IOP Conf Ser Mater Sci Eng.* 2016;149:012043. doi: 10.1088/1757-899X/149/1/012043
21. John LK, Murugan R, Singamneni S. Impact of quasi-isotropic raster layup on the mechanical behaviour of fused filament fabrication parts. *High Perform Polym.* 2022;34(1):77-86. doi: 10.1177/09540083211041954
22. John LK, Ramu M, Singamneni S, Binudas N. Strength evaluation of polymer ceramic composites: A comparative study between injection molding and fused filament fabrication techniques. *Prog Addit Manuf.* 2025;10(1):339-347. doi: 10.1007/s40964-024-00626-9
23. Pourhajrezaei S, Abbas Z, Khalili MA, *et al.* Bioactive polymers: A comprehensive review on bone grafting biomaterials. *Int J Biol Macromol.*

2024;278:134615.
doi: 10.1016/j.ijbiomac.2024.134615
24. Farag MM. Recent trends on biomaterials for tissue regeneration applications. *J Mater Sci.* 2023;58(2):527-558.
doi: 10.1007/s10853-022-08102-x
25. Cao S, Bo R, Zhang Y. Polymeric scaffolds for regeneration of central/peripheral nerves and soft connective tissues. *Adv NanoBiomed Res.* 2023;3(3):2200147.
doi: 10.1002/anbr.202200147
26. O'brien FJ. Biomaterials and scaffolds for tissue engineering. *Mater Today.* 2011;14(3):88-95.
doi: 10.1016/S1369-7021(11)70058-X
27. Lasprilla AJ, Martinez GA, Lunelli BH, Jardini AL, Maciel Filho R. Poly-lactic acid synthesis for application in biomedical devices-A review. *Biotechnol Adv.* 2012;30(1):321-328.
doi: 10.1016/j.biotechadv.2011.06.019
28. Bos RRM, Rozema FB, Boering G, *et al.* Degradation of and tissue reaction to biodegradable poly (L-lactide) for use as internal fixation of fractures: A study in rats. *Biomaterials.* 1991;12(1):32-36.
doi: 10.1016/0142-9612(91)90128-W
29. Biswal T. Biopolymers for tissue engineering applications: A review. *Mater Today Proc.* 2021;41:397-402.
doi: 10.1016/j.matpr.2020.09.628
30. Sagadevan S, Schirhagl R, Rahman MZ, *et al.* Recent advancements in polymer matrix nanocomposites for bone tissue engineering applications. *J Drug Deliv Sci Technol.* 2023;82:104313.
doi: 10.1016/j.jddst.2023.104313
31. Ning F, Cong W, Qiu J, Wei J, Wang S. Additive manufacturing of carbon fiber reinforced thermoplastic composites using fused deposition modeling. *Compos B Eng.* 2015;80:369-378.
doi: 10.1016/j.compositesb.2015.06.013
32. Chou YC, Lee D, Chang TM, *et al.* Development of a three-dimensional (3D) printed biodegradable cage to convert morselized corticocancellous bone chips into a structured cortical bone graft. *Int J Mol Sci.* 2016;17(4):595.
doi: 10.3390/ijms17040595
33. Warnke PH, Seitz H, Warnke F, *et al.* Ceramic scaffolds produced by computer-assisted 3D printing and sintering: Characterization and biocompatibility investigations. *J Biomed Mater Res B Appl Biomater.* 2010;93(1):212-217.
doi: 10.1002/jbm.b.31577
34. Hedayati SK, Behravesh AH, Hasannia S, Saed AB, Akhoundi B. 3D printed PCL scaffold reinforced with continuous biodegradable fiber yarn: A study on mechanical and cell viability properties. *Polym Test.* 2020;83:106347.
doi: 10.1016/j.polymertesting.2020.106347
35. Chen SY, Cho YC, Yang TS, *et al.* A tailored biomimetic hydrogel as potential bioink to print a cell scaffold for tissue engineering applications: Printability and cell viability evaluation. *Appl Sci.* 2021;11(2):829.
doi: 10.3390/app11020829
36. Laeng J, Khan ZA, Khu SY. Optimizing flexible behaviour of bow prototype using Taguchi approach. *J Appl Sci.* 2006;6(3):622-630.
doi: 10.3923/jas.2006.622.630
37. Liu X, Zhang M, Li S, Si L, Peng J, Hu Y. Mechanical property parametric appraisal of fused deposition modeling parts based on the gray Taguchi method. *Int J Adv Manuf Technol.* 2017;89:2387-2397.
doi: 10.1007/s00170-016-9263-3
38. Lee BH, Abdullah J, Khan ZA. Optimization of rapid prototyping parameters for production of flexible ABS object. *J Mater Process Technol.* 2005;169(1):54-61.
doi: 10.1016/j.jmatprotec.2005.02.259
39. Deng X, Zeng Z, Peng B, Yan S, Ke W. Mechanical properties optimization of poly-ether-ether-ketone via fused deposition modeling. *Materials* (*Basel*). 2018;11(2):216.
doi: 10.3390/ma11020216
40. Dong G, Wijaya G, Tang Y, Zhao YF. Optimizing process parameters of fused deposition modeling by Taguchi method for the fabrication of lattice structures. *Addit Manuf.* 2018;19:62-72.
doi: 10.1016/j.addma.2017.11.004
41. Fitzharris ER, Watt I, Rosen DW, Shofner ML. Interlayer bonding improvement of material extrusion parts with polyphenylene sulfide using the Taguchi method. *Addit Manuf.* 2018;24:287-297.
doi: 10.1016/j.addma.2018.10.003
42. Cimbala JM. *Taguchi Orthogonal Arrays.* Pennsylvania: Penn State University; 2014. p. 1-3.

Received: April 7, 2025
Revised: May 25, 2025
Accepted: May 26, 2025
Available online: June 20, 2025